

# DESIGNING A DO-IT-YOURSELF UNMANNED AERIAL VEHICLE FOR ARCTIC RESEARCH PURPOSES AND PROVING ITS CAPABILITIES BY RETRIEVING SNOW DEPTH VIA STRUCTURE-FROM-MOTION



**D. Kramer<sup>1,2\*</sup>, J. Meloche<sup>1,2</sup>, A. Langlois<sup>1,2</sup>, D. McLennan<sup>3</sup>, B. Chapdelaine<sup>4</sup>, C. Gauthier-Barrette<sup>1</sup>, A. Royer<sup>1,2</sup> and P. Cliche<sup>1</sup>**

<sup>1</sup> Centre d'applications et de recherches en télédétection (CARTEL), Université de Sherbrooke, Quebec, Canada

<sup>2</sup> Centre d'études nordiques, Quebec, Canada

<sup>3</sup> Polar Knowledge Canada, Canadian High Arctic Research Station, Cambridge Bay, Nunavut, Canada

<sup>4</sup> Institut interdisciplinaire d'innovation technologique, Sherbrooke, Quebec, Canada

\* [Daniel.kramer@usherbrooke.ca](mailto:Daniel.kramer@usherbrooke.ca)

## Abstract

Unmanned Aerial Vehicles (UAVs) have become commonplace in many scientific applications, including operations in harsh environmental conditions. However, off-the-shelf UAVs capable of this type of work are very expensive and offer limited flexibility for custom payloads. Cost-effective and customized UAV system capabilities for site exploration, mapping, surveying and atmospheric profiling in the Arctic are needed. The goal of this project was to develop a do-it-yourself (DIY) platform from simple, pre-manufactured components capable of flight operations in extreme arctic and polar winter conditions. This approach provides the flexibility to fly a range of sensor payloads for different applications and allows for easy on-site modifications and low-cost repairs. A highly customized payload example is the Ka-band radar used by the research team (circa 700 grams (g), 200 x 130 x 150 millimetres (mm)) and more

common examples are cameras like the MAPIR Survey 3 (circa 50 g, 59 x 41.5 x 36 mm). Where some manufacture warranties (like senseFly) require the UAV to be sent in even for minor repairs, on-site modifications and repairs can keep the costs to operation a DIY UAV low.

To meet this goal, different components were tested under controlled conditions to verify their functionality in extreme cold temperatures and their compatibility with devices used during fieldwork. To further validate the scientific capability of the DIY UAV system design, a small area near Cambridge Bay, Nunavut, Canada was surveyed to retrieve snow depth via structure-from-motion (SfM). This produced a snow depth map with a horizontal resolution of 6 cm. The calculated snow depth, with a root mean square error (RMSE) of 16 centimetres (cm) (13 cm without points

*Suggested citation:*

Kramer, D., Meloche, J., Langlois, A., McLennan, D., Chapdelaine, B., Gauthier-Barrette, C., Royer, A., Cliche, P. 2019. Designing a Do-It-Yourself Unmanned aerial Vehicle for Arctic research purposes and proving its capabilities by retrieving snow depth via structure-from-motion. *Aqhaliat* 2019, Polar Knowledge Canada, p. 43-62. DOI: 10.35298/pkc.2019.05

over vegetation), matches values found in the literature that were retrieved at lower latitudes using much more expensive platforms. The main UAV type studied in this project can operate safely in temperatures as low as -40 degrees Celsius (°C) and at even colder temperatures, though with slightly reduced capabilities. The DIY UAV design is currently limited to a maximum wind speed of 10 metres per second (m/s), including a large safety margin. Next steps include the development of a rotary-wing aircraft to carry a radar system capable of snow and ice profiling and a fixed-wing aircraft to fly in wind speeds over 10 m/s.

## Introduction

Unmanned Aerial Vehicles (UAVs) are frequently used in many geoscientific fields (Anderson et al., 2019) and arctic research applications (Chudley et al., 2019). Arctic scientific applications will greatly benefit from the possibilities that UAVs offer. For example, traditional methods of snow depth acquisition (Langlois et al., 2010), like manual measurements with an avalanche probe or digging a snow pit, are time consuming and limited to a small area which leads to representativeness problems. UAVs can cover a much larger area (Jo and Kwon, 2019), avoid spatial interpolation, and can easily track changes in an area over time (e.g., vegetation). Furthermore, by better representing local processes (snow distribution versus roughness/topography) that are difficult to represent with the coarser spatial resolution of satellite imagery, UAVs can also reduce modelling uncertainties (Rutter et al., 2014).

UAV technology is developing quickly and usability is improving. Nevertheless, the harsh environmental conditions of polar regions put considerable strain on aircraft that can be challenging for simple, off-the-shelf solutions (DJI, 2015). In addition, these systems are often closed and don't allow parameter modifications or easy on-site maintenance and repair. Advanced systems, like the senseFly eBee or the Microdrones md4-

3000, can handle harsh environmental conditions better, but their price tags, which can exceed US\$ 30 000, can be restrictive. Furthermore, these advanced systems do not usually allow for modifying payloads or attaching systems or sensors for specific scientific requirements. The alternative is the do-it-yourself (DIY) approach. This makes it possible to make specific alterations to an aircraft for the desired task. It also allows for easy repairs and modifications during field campaigns to address problems that arise. An additional benefit is the ability to re-use the electronics in different UAVs, which significantly lowers the price for new aircraft as a new frame can usually be acquired for under US\$ 200.

The philosophy behind the technical part of this paper is to construct simple and low-cost UAVs that can operate in the Arctic and meet scientific standards in surface state retrievals accuracy. Care was taken to avoid complicated procedures with airspace authorities, in this case Transport Canada (TC). Site selection and tasks were designed to meet all TC exemptions (e.g., distance to built-up areas, airspace class, and flight altitudes and distances). While this design limits flying opportunities, it avoids the wait time associated with requesting and obtaining Special Flight Operations Certificates (SFOCs)<sup>1</sup> and allows for last minute science-based decisions on flight needs.

To show that this approach can meet scientific standards for data acquisition this paper aims to provide:

- Technical details of the project's approach, including hardware and software information, and lessons learned from past campaigns; and
- An example of application by retrieving snow depth data using structure-from-motion (SfM), validated using field measurements.

Consequently, the article is divided into two main sections: first, a description of the technical

<sup>1</sup>The regulations from Transport Canada changed as of June 1 2019. The restrictions in place during the project are no longer in effect. The new regulations that will be in effect for future flight missions can be found at: <https://www.tc.gc.ca/en/services/aviation/drone-safety/new-rules-drones.html>.

solutions, experiments, and experiences of operating a UAV in the Arctic, and second, a demonstration of the capabilities of the DIY-UAV system design in retrieving snow depth in the Arctic.

## UAV development and overview

This section discusses the configurations of the different aircrafts and the environmental influences on the materials and electronics. Some experiments were conducted in a controlled environment (weather chamber), whereas other tests and observations were done during fieldwork. Notably, operating near the geomagnetic pole (e.g., Cambridge Bay, 1500 kilometres (km)) while using a magnetometer can cause problems flying UAVs. Manual flight may be necessary, as most UAVs use a magnetometer to determine the heading while flying on autopilot. Rotary-wing or multicopter aircrafts strongly rely on magnetometers for orientation because of the ability to hover or fly with low speed. In comparison, fixed-wing aircrafts can estimate heading solely from the tracking of the previous global positioning system (GPS) point navigation (Ader and Axelsson, 2017). Cimoli et al., (2017) used a rotary-wing in the Arctic and report briefly on their experience: *“GPS and compass navigation are compromised at high latitude (due to magnetic field interference) [...] It is recommended that pilots be prepared to perform the survey in manual mode.”*

From personal experiences and reports from colleagues, fly-aways on random trajectories occurred with older versions of DJI products. With newer versions, the autopilot switches automatically to *altitude hold/manual mode* when trying to fly in *full automatic/GPS mode*. While manual flying is possible, very advanced flying skills are required to obtain good measurements from the sensors carried on the UAV. For instance, if a SfM approach is planned, angle, speed, and camera timing must be controlled to provide sufficient overlap between the photographs. An alternative is to record video instead of photographs. However, this requires more intensive post-processing and lowers the resolution of the images.

For the purpose of this project, it was decided to only use GPS for navigation on the aircraft, with additional reliance on autopilot calibration. For this reason, the DIY UAV design is a fixed-wing frame. The autopilot can be used without a magnetometer and fixed-wing aircraft are better suited for longer flight time, which is good for mapping. A DJI Phantom 3 Professional aircraft was also used in manual mode for comparison on several occasions.

## Batteries

The following section describes the battery tests that were conducted to identify potential flying times in different temperature conditions. The focus of this testing was to better understand battery performance, e.g., how long will a battery last on a certain load, independent of UAV-type, wind-speed, or other factors. Knowing battery-performance is an important aspect of planning flight missions as it impacts decisions on parameters like flight-lines, cover area and expected flight time under the prevailing weather conditions. For the fleet used in this project, Lithium polymer batteries were selected. These batteries are widely used for UAVs, as they “offer the optimal compromise of moderate specific energy, high specific power, and high cycle life” (Abdilla et al., 2015; Mulgaonkar et al., 2014). The long-term goal is to cover similar distances as commercially available UAVs (e.g., 1000 square metres (m<sup>2</sup>), while being able to switch payload on site.

## Test set-up

Power consumption was estimated by analyzing a real flight log from a fixed-wing aircraft (BlitzRCWorks Skysurfer Pro, see Figure 5, left) carrying no payload. The flight took place under good conditions (< 10 metres per second (m/s) wind, around 0 degrees Celsius (°C)). The amperage (A) used during the flight varied between 1 A and 25 A, and most power was consumed during take-off and climb. When gliding, almost no power was needed, so an average of load of 16 A was calculated to replicate ‘normal’ flight consumption. Table 1 lists the batteries tested. The constant

Table 1: Batteries used in experiments. All batteries have 4 cells.

Battery	Milliamperes per hour (mAh)	Volts (V)	Watts per hour (Wh)	Constant Discharge C-Rating	Peak Discharge C-Rating
Phantom 3	4480	15.2	68	N.A.	N.A.
Nano-tech 4.0 (Turnigy)	4000	14.8	59.2	30 C	40 C (10 s)
Multistar 4.0 (Turnigy)	4000	14.8	59.2	12 C	24 C
Multistar 5.2 (Turnigy)	5200	14.8	76.96	12 C	24 C

discharge refers to the rate at which the battery can continuously discharge itself without being damaged. The peak discharge characterises the battery's ability to discharge a higher amount than the constant discharge over a short period of time. The schematic of the experiment is shown in Figure 1.

### Test types and protocol

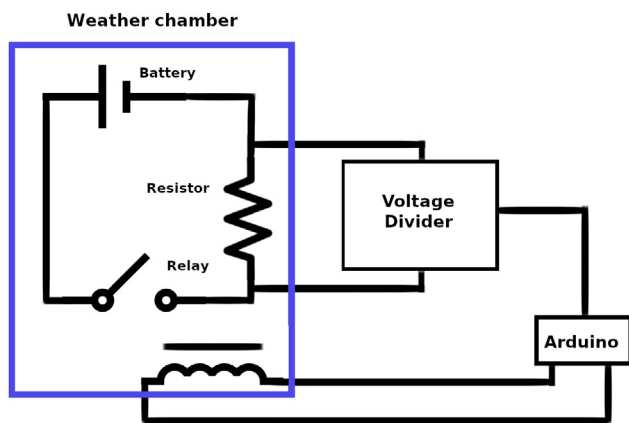


Figure 1: Experimental set-up.

Three types of tests were conducted.

**Test type 1:** During the test, a constant high load (16 A) was applied at a specific temperature. Before, the test the battery was kept at room temperature to simulate keeping a battery warm (e.g., near body) while being out in the field.

**Test type 2:** Before, the test the battery was frozen to a specific temperature to simulate the battery being transported on the field, without

temperature protection. As in Test type 1, the applied load was 16 A.

**Test type 3:** During the test, a small low load (1 A) was applied to investigate the effect of cold temperatures on battery life. Before, the test the battery was kept at room temperature.

The following protocol was used to standardize the tests:

1. All parts of the circuit are connected, and two freezers are used. One is held at a constant temperature, in which the battery is inserted. The other was set to  $-80\text{ }^{\circ}\text{C}$  to cool the load (several resistors). The resistors are controlled by an Arduino microcontroller, which is connected to a relay. The resistors are used to simulate the load applied during a flight.
2. During test types 1 and 2, the freezer is set and kept at a desired temperature. The temperature ranges from  $-20\text{ }^{\circ}\text{C}$  to  $-40\text{ }^{\circ}\text{C}$ , which reflects normal conditions during fieldwork. The tests were conducted at  $10\text{ }^{\circ}\text{C}$  intervals. Results from test type 3 ranged from  $+4\text{ }^{\circ}\text{C}$  to  $-40\text{ }^{\circ}\text{C}$ .
3. A fully charged battery was placed in the freezer and connected to the circuit. Batteries were always placed in the same position/orientation/part of the freezer to avoid random factors influencing the results.
4. At the start, after about 350 seconds (s), and at the end of each test, the resistance (R) was measured to verify that the load was constant and there was no resistor malfunction.

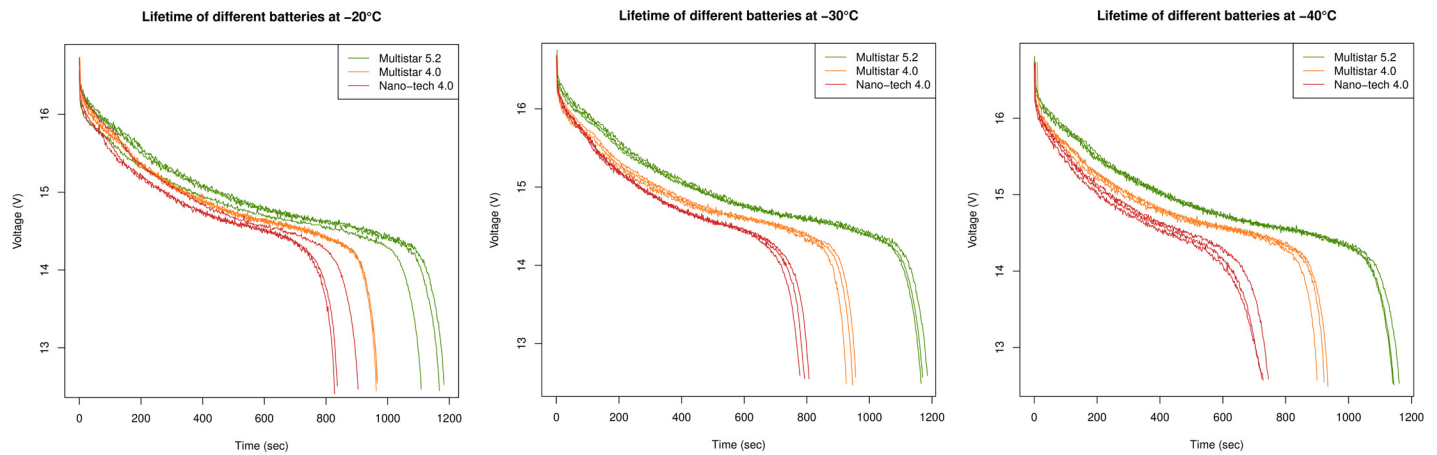


Figure 2: Comparison of three different batteries at three different temperatures.

5. To prevent battery damage, the system automatically shut down when the battery reached 12.6 volts (V) (3.15 V per cell). Further explanation follows in the Results section.
6. For each setting, the test was repeated 3 times per battery (except for test type 3, further explanation follows below).

## Test Results

For all tests, R was in a range between 0.93 and 0.98 ohm ( $\Omega$ ). Therefore, the load during the tests was as planned.

**Test type 1:** Figure 2 compares the discharge of the three different battery types at three different temperatures. The Phantom 3 battery heated up so

much in the first test, that further testing with this battery was discontinued. In repeated testing, the performance of each battery was relatively similar, though there are visible differences between battery types. As batteries lose strength over time, it is important to note that no record was kept of the battery cycles. The Multistar 4.0 and 5.2 were almost new, and the Nano-tech 4.0 had been in use for about two years.

At 5200 milliampere per hour (mAh), the Multistar 5.2 had the highest capacity, while at 4000 mAh, the Multistar 4.0 and Nano-tech 4.0 had the same capacity. The Multistar 4.0 and Nano-tech 4.0 have different C-ratings (maximum safe current draw)—the Nano-tech rating is higher (25 to 50 °C) than the Multistar 4.0 (12 °C).

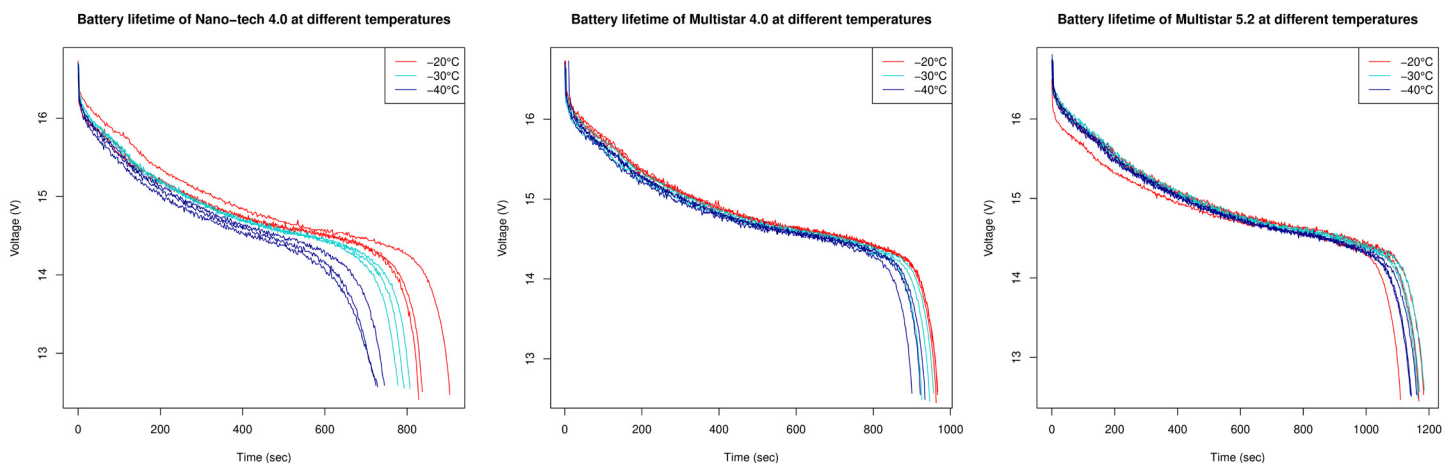


Figure 3: Results for three different battery types at three different temperatures.

All three batteries had a sharp decline in capacity at about 14.5 V. In Figure 3, each battery type is presented in its own graph, which also show the different temperatures. The Nano-tech 4.0 (left graph) is the most sensitive to temperature. It loses about 3 minutes of operational time at  $-40\text{ }^{\circ}\text{C}$  (7.35 minutes (min)) in comparison to  $-20\text{ }^{\circ}\text{C}$  (10.28 min). The Multistar 4.0 (middle graph) loses just over 1 minute of time at  $-40\text{ }^{\circ}\text{C}$  (11 min) in comparison to  $-20\text{ }^{\circ}\text{C}$  (12.16 min). The Multistar 5.2 (right graph) loses almost exactly 1 minute of time between  $-20\text{ }^{\circ}\text{C}$  and  $-40\text{ }^{\circ}\text{C}$ . In all three cases, the results represent mean values over the three tests performed with each battery at each temperature.

**Test type 2:** The first test was conducted at  $-20\text{ }^{\circ}\text{C}$  and the battery was exposed to the cold for 30 min. As the load was applied, the voltage immediately dropped under 12.6 V. As this was the upper end of the temperature test, no further tests were conducted. Only the Nano-tech 4.0 was tested. It was assumed that other LiPo-batteries, though maybe of a slightly different chemical composition, would react in a similar way.

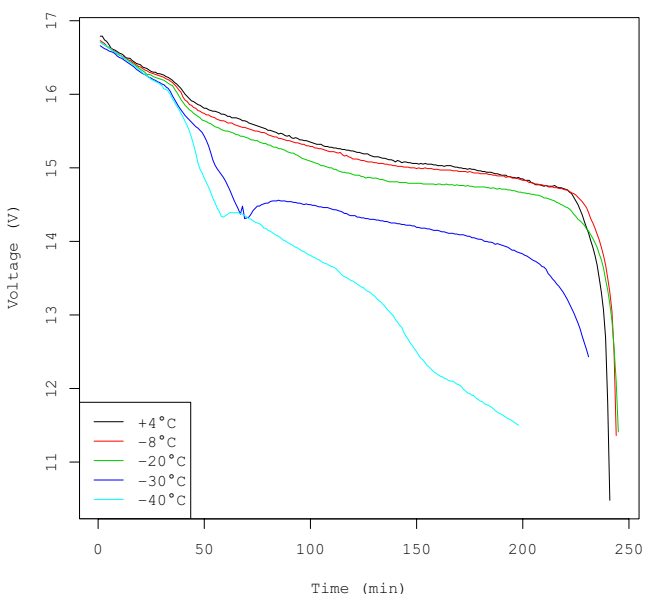


Figure 4: Long-term exposure of a battery (the Nano-tech 4.0) to different temperatures. Note the distinct drop of discharge capacity at around 50 minutes for temperatures below  $-30\text{ }^{\circ}\text{C}$ .

**Test type 3:** The protocol described in the previous section was repeated at five different temperatures with the Nano-tech 4.0 (see Figure 4). Notably, the test at  $-8\text{ }^{\circ}\text{C}$  had to be conducted under real conditions outside at night with variable temperatures. The equipment at the time of the test was not able to cool to a temperature above  $-20\text{ }^{\circ}\text{C}$ . For the temperature at  $+4\text{ }^{\circ}\text{C}$ , a conventional fridge was used while the other tests were performed in a controlled weather chamber. Results depicted in Figure 4 suggest that the impact of temperature on the discharge capability is rather low at  $-20\text{ }^{\circ}\text{C}$ , but a significant change can be observed at lower temperatures (at about 50 minutes into the test).

## Discussion

**Test type 1:** Battery age appears to play an important role. The Nano-tech 4.0 significantly underperforms the others, despite having specifications that are comparable to the Multistar 4.0. Table 2 presents the average operation time for each battery at each temperature (average of three tests). Voltage was measured and recorded throughout the test as well as the time at which the battery reached 14.50 V for the first time. The results are similar to values found in the literature, e.g., Winslow et al. (2016). After this interval, battery capacity drops sharply. To avoid damage to the battery, its voltage should never drop below 12 V, although an extra 0.5 V buffer was built into the project design. The 12 V is a combined result from 4 cell batteries, each with a lower limit of 3 V. The typical cell has an operational range from 2.3

Table 2: Time in seconds until the battery reached 14.50 V. Shortly after this value, voltages for all batteries drop sharply until reaching the cut-off limit of 12.5 V. The displayed value is the mean of 3 tests.

Temperature	Nano-tech 4.0	Multistar 4.0	Multistar 5.2
$-20\text{ }^{\circ}\text{C}$	617 s	730 s	897 s
$-30\text{ }^{\circ}\text{C}$	537 s	702 s	897 s
$-40\text{ }^{\circ}\text{C}$	441 s	654 s	832 s

to 4.2 V (Salerno and Korsunsky, 1998), but the 3 V is a widely used rule-of-thumb as the V-drop is not linear.

This test allows us to better estimate flight times, assuming a constant load. The load used for testing was high enough to underestimate rather than overestimate flight times. As mentioned earlier, the difference between the Nano-tech 4.0 and the Multistar 5.2 (and to some degree the Multistar 4.0) is almost 3 minutes when compared at -20 °C and -40 °C, respectively. Since the Nano-tech 4.0 is by far the oldest battery, this finding suggests it is reasonable to repeat this type of experiment as a 'good habit' with older batteries before deployment to ensure airworthiness and estimate discharge-time. The purchase of a new battery is not a big expense and could significantly increase safety and flight time.

**Test type 2:** Due to the different chemical compositions, this value might differ for each battery type/manufacturer. However, the test results indicate the best practise is to keep the batteries warm until the last moment. Since the research sites are usually  $\geq 30$  minutes away from accommodations, measures must be taken to ensure batteries remain warm until use.

**Test type 3:** A difference was found between the voltage measurements taken at the end of the experiment and those taken once the battery was removed from the weather chamber and allowed to warm up. Ideally, the battery should be tested under no load in both conditions. The impedance of the battery increases as the temperature lowers (Wang, 2015). This phenomenon demonstrates that a temperature drop causes a loss of discharge capacity, which is mainly caused by an increase of the internal resistance of the battery. This lowers the discharge rate and capacity (Wang, 2015). From a practical standpoint, the significant loss of discharge capacity between -20 °C and -30 °C is not particularly relevant for the purposes of this design project. Since the typical flight times are under 50 minutes and the typical load draw from the battery is higher, the battery would be empty before the cold had an impact.

## Frames

Various commercially available platforms were tested for the design project including two DIY fixed-wing platforms (both motor glider) and one off-the-shelf rotary-wing platform. To begin UAV operations, test flights were conducted as part of various campaigns in Southern Ontario, Nunavut, and Quebec. The initial price tag for our DIY system was about US\$ 1 250, which is comparable to the cost of a low-end, off-the-shelf solution like the DJI Phantom 3 Professional.

The DJI Phantom 3 Professional was used to represent an off-the-shelf system and well-known platform. While it is a different type of UAV (rotary-wing) that cannot be compared in every aspect to fixed-wing frames, it serves as a benchmark for testing. The DJI Phantom 3 Professional produced results quickly and was a good tool to start UAV operations. This device was used in the Bay of Quinte region (Southern Ontario, Canada; 44°43'06.5370"N, 77°35'46.6923"W) for a snow mapping campaign in 2017 and in the Greiner Lake Watershed near Cambridge Bay (Nunavut, Canada; 69°14'11.78"N, 104°52'55.10"W) during a summer campaign in 2018. During the snow mapping campaign in the Bay of Quinte, there were a few issues with the DJI Phantom 3 Professional, but it was able to fly using the autopilot setting. Unfortunately, this was not possible in the Greiner Lake Watershed summer campaign. We assume the relative proximity to the magnetic North Pole interfered with the magnetometer readings needed for orientation and forced the pilot to fly manually.

The first DIY platform built and tested was the BlitzRCWorks Skysurfer Pro. This aircraft has no payload bay and required customization. The flying weight of the aircraft is stated as 650 grams (g) by the manufacturer. The customization included adding 117 g for the camera (GoPro 6) and 485 g for a larger battery. Following this, the take-off weight was 1 252 g and put the engine to the limit of its propulsion capabilities. The customized design was able to retrieve data and was used on a winter and a summer campaign in Cambridge Bay, as well as



Figure 5: From left to right: the BlitzRCWorks Skysurfer Pro, Finwing Penguin, interior of the Finwing Penguin, and the DJI Phantom 3 Professional.

on test flights in the Sherbrooke area (Quebec, Canada).

While the build was easy, the test flights identified a few problems. Notably, the Electronic Speed Controller (ESC) on the BlitzRCWorks Skysurfer Pro did not work below 0 °C. This finding led to testing all electronic components in the weather chambers instead of focusing solely on battery discharge abilities. In addition, the aircraft has a very limited payload capacity and, lacking previous experience, the most powerful battery that would fit in the aircraft was used to ensure sufficient power during flight. The advantages of the BlitzRCWorks Skysurfer Pro platform are its low price (around US\$ 75 for the frame) and its gliding properties. It is easy to fly and a great platform to unexperienced pilots. However, glider planes have problems in higher wind speeds (the maximum wind speed deemed safe in testing was 10 m/s).

The second DIY platform built and tested was the Finwing Penguin (about US\$ 200). This aircraft has a designated payload bay (with some modification it can fit a Sony A6000, weight: 468 g, dimension: 120 x 67 x 45 mm) and can carry up to 900 g payload (manufacturer's specifications). The aircraft all-up weight (AUW) shall not exceed 2.4 kilograms. The aircraft was easy to build and can be done in a short amount of time. Compared to the BlitzRCWorks Skysurfer Pro, which was also at its AUW, the Finwing Penguin felt more comfortable in the air. Its hardware is more robust than the

BlitzRCWorks Skysurfer Pro and the aircraft performed better for the testing purposes. As a motor glider, strong winds remain a problem, but it was still comfortable to fly in 10 m/s (wind in 2 m height, not measured higher up at an altitude of 50 to 70 m) in the Fly-By-Wire-mode (assisted flying) and was acceptable in manual flight mode.

A summary of the pros and cons of the various DIY platforms tested can be found in Table 3, with pictures of the different platforms in Figure 5.

### Electronic components

The electronic components are exposed to cold conditions during transport to the site and the

Table 3: Pros and cons of the commercially available UAV platforms tested.

	DJI Phantom 3 Professional	BlitzRCWorks Skysurfer Pro	Finwing Penguin
<b>Pro</b>	Off-the-shelf Price/perf. ratio Quick results	Cheap Easy to fly	Easy to fly Payload bay Stronger engine
<b>Con</b>	Closed system Difficulties in cold temperatures	Limited payload capacity Underpowered Difficulties in wind	Slightly more expensive Limited payload capacity

flights themselves. To ensure a working aircraft in cold conditions, all electronic components were tested in a controlled freezer. This test was separate from the battery test, since the batteries are stored in warm conditions. For the experiments, the electronics parts were left in the freezer at the indicated temperature for a minimum of one hour. Figure 6 shows the wiring of the electronic components tested.

This test was not conducted for the DJI Phantom 3 Professional (the benchmark, off-the-shelf platform), as operational ranges were provided by the manufacturer (DJI, 2015). Table 4 lists the X-UAV Talon for reference, however this platform has not yet been used in fieldwork. Cameras were not tested either, as they are not critical for safe flights.

## Results and discussion

As shown in Table 4, the operational temperature range of the aircrafts differ. As the BlitzRCWorks Skysurfer Pro stopped operating at  $-5^{\circ}\text{C}$ , tests were not continued below this limit. Similarly, tests for the Finwing Penguin and X-UAV Talon were not conducted above  $-15^{\circ}\text{C}$ , as they had already been shown to be operational down to  $-40^{\circ}\text{C}$  and with limitations to  $-50^{\circ}\text{C}$ .

The BlitzRCWorks Skysurfer Pro can only be used in above-zero temperatures, as the ESC stops working below  $0^{\circ}\text{C}$ . The ESC directly controls the engine and thus is essential for automated flight. Manual flights during fieldwork are still possible and have been conducted between  $-20^{\circ}\text{C}$  and  $-30^{\circ}\text{C}$ . The Finwing Penguin and X-UAV Talon have proven to be fully operational down to  $-40^{\circ}\text{C}$ , though at  $-50^{\circ}\text{C}$  the servo motors that control pitch, yaw, and roll had a reduced range of movement. Based on these results, both aircrafts can be flown down to temperatures around  $-40^{\circ}\text{C}$ . This test also showed that the other components like GPS, telemetry module, radio receiver, and autopilot (in this case Pixhawk 2) are operational in the tested temperatures.

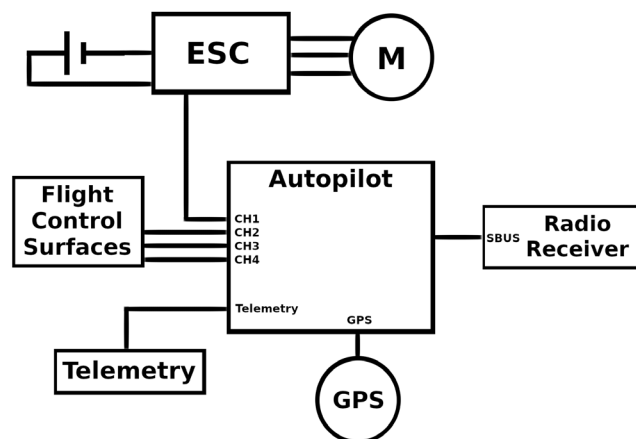


Figure 6: Wiring diagram of the electronic components of the DIY UAV designs.

## Mounted sensors

To date, only two types of cameras have been used in the DIY UAV system design. The main camera system used during fieldwork is a GoPro 6. In addition to having a robust, waterproof design, the GoPro 6 can be used in temperatures around  $-30^{\circ}\text{C}$  for the duration of two flights and preparation (about 1 hour). The other camera used is the standard camera on the DJI Phantom 3 Professional. This was used during summer missions and produced reliable results, which are presented in the next chapter. A small camera (MAPIR Survey 3, circa 50 g, 59 x 41.5 x 36 mm) and a small frequency-modulated continuous wave (FMCW) Ka-band radar system (circa 700 g, 200 x 130 x 150 mm) will be mounted on the DIY UAV design in 2019–2020. The radar system has already been used during fieldwork in temperatures around  $-40^{\circ}\text{C}$  and has shown no signs of cold-related limitations. It will be used for UAV-based snow and ice thickness retrievals (Pomerleau et al., 2018).

## Summary and outlook

The ability to customize specific UAVs for all needs and to change frames and re-use electronics make the DIY approach good for medium-sized research groups that can afford the manpower to build a DIY system. Another advantage of the DIY approach is high independence in the field if repairs and troubleshooting are required. With new technology

Table 4: Test results for electronic components in extreme cold temperatures. The 'X' means that the electronic device failed the test, the check mark that the test was successful, and a check mark in brackets that the electronic device still worked, but at a reduced capacity.

Model	Temp. (°C)	ESC / arming	Servo	Comment
BlitzRCWorks Sky Surfer Pro	0	√	√	
	-5	X	√	
	-10	X	√	
	-15	X	√	
	-20	X	√	
	-30	X	√	
	-40	Na	Na	Tests were not continued
	-50	Na	Na	
Finwing Penguin	-10	Na	Na	Tests not conducted
	-15	Na	Na	
	-20	√	√	
	-30	√	√	
	-40	√	√	
	-50	√	(√)	Servos not moving full range
X-UAV Talon	-10	Na	Na	Tests not conducted
	-15	Na	Na	
	-20	√	√	
	-30	√	√	
	-40	√	√	
	-50	√	(√)	Servos not at full range

emerging, frames will get outdated or improved. Being able to adapt to these changes at low cost for each UAV system is one of the strongest advantages of the DIY approach, for more info on our build and electronics, see appendix E.

### General operations

- To further customize payloads and general aspects of the 'interior' design, the DIY UAV system design uses a 3D printer. Many parts are available online or can be designed quickly. While polyactic acid was found to be an adequate material in most circumstances, an ecofriendly acrylonitrile butadiene styrene

material was used for most purposes. The 3D-printed plastic parts were less brittle than expected.

- To reach the research sites it takes  $\geq 30$  minutes by snowmobile. These trips are hard on any material. Since experiments with heating the aircraft did not work well, the current best practise is to allow the frame to cool down and simply cushion it for the hard ride. Since some glues (e.g., underside of Velcro-strips) lose adhesiveness in the cold, it is better to use mechanical mounting where possible.

- Experiments also showed it is important to keep the batteries warm until the last moment. Initially, 4000 mAh batteries were used. After conducting the test series, 5200 mAh batteries were mainly used. This switch increases the weight and reduces the payload capacity for sensors, but the additional flight time makes up for this.
- While hard landings can occur, surface scratches can be repaired easily with Tuck Tape, superglue, and epoxy.

### Future work and development

In the early stages of the development, it was necessary to take manual control of the aircraft several times (ESC-failure, autopilot settings, etc.). During campaigns in spring and summer 2019, the problems have been solved and the autopilot is working great. For the purpose of flight operations in polar winter conditions, fixed-wing UAVs will be used for most missions, unless specific requirements are needed (e.g. hovering and low altitude flights for radar measurements). Plans to build a quadcopter in late 2019 will enable flights with the new FMCW radar system. Another future development will be to increase payload flexibility.

Work is also currently underway to develop a mounting system that will support both DIY and off-the-shelf systems with a small adapter unique to the UAV. Being able to mount independent payloads on any system will allow scientists to conduct research most efficiently. As of 2019, several reasonably priced, off-the-shelf UAVs (e.g., the DJI Phantom 4 RTK and DJI Matrice 600 Pro, which are both under US\$ 10 000) have entered the market. The great advantage of newer off-the-shelf UAVs is the plug-and-play capability. This enables unexperienced users to achieve reasonable results in very short time. However, unexperienced users typically have a lesser understanding of how the UAV works and limited manual flight experience. Since operations take place in a challenging environment, that adds a lot of stress due to its natural conditions, this is a concern.

## UAV application: snow depth retrieval

This section demonstrates the capabilities of the project's DIY UAV system design in retrieving snow depth in the Arctic. The technique used for retrieving snow depth from UAV is based on the structure-from-motion (SfM) workflow described below. This technique is widely used by scientists and surveyors (Fernandes et al., 2018). From this workflow, precise topographic maps are obtained and can be used for many applications, including temporal evolution of landslides (Turner et al., 2015), and reconstruction of an historical building (Murtiyoso et al., 2017).

### Introduction

Snow depths are derived from the difference between two topographic maps. The most accurate way to derive snow depths is by using a digital surface model (DSM), where one surface model is acquired in summer (snow-off condition) and one in the winter (snow-on conditions). This technique has been used for snow depth mapping in alpine regions (e.g., by Bühler et al., 2016; De Michele et al., 2016; and Eckerstorfer et al., 2015). However, very few studies are available for arctic regions:

- Nolan et al., (2015) mapped snow depth in Alaska by aircraft, using SfM with a consumer grade camera. They were able to achieve 10 cm precision on snow depth for arctic snow where influences of vegetation and other factors were minimized.
- Cimoli et al., (2017) mapped snow depth in Svalbard and Greenland with UAVs but used a terrestrial DSM to acquire snow-off conditions in summer. They measured a range root mean square error for multiple site from 5 to 18 cm.
- Bühler et al., (2016) mapped snow depth in alpine terrain with UAVs. Their study shows that SfM works for snow depth in alpine terrain to an acceptable accuracy, with an RMSE of 0.07 m to 0.15 m in meadows and an RMSE of less than 0.3 m in areas with bushes or tall grass.

The SfM workflow uses multiple images to create a three dimensional (3D) reconstruction. The first step is to find features (or tie points) that appear in multiple images. These points are found by using the Scale Invariant Feature Transform (SIFTs) detection algorithm (Lowe, 2004). An initial 3D reconstruction can be done using estimated camera parameters (position and orientation), which yields to a 3D point cloud. This process is optimized by using Bundle Adjustment (Granshaw, 1980).

### Snow depth retrieval application

For the purpose of this project, ground control points (GCP) with well-known positions were used to refine camera parameters and provide a GPS datum for the point cloud. This project used Agisoft Photoscan version 1.4.3 and the GCPs were acquired using a differential GPS (dGPS) system that consists of a Trimble Net R9 with Trimble Zephyr Geodetic antenna as a base station, and a u-blox receiver as a rover. A base station point was measured from 5 hours static acquisition with a sampling interval of 1 second. Then the position was refined using Precise Point Positioning (PPP) from Natural Resources Canada.

The relative accuracy of the targets is 0.5 cm on the X-/Y-axes and 1 cm on the Z-axis. This is the accuracy from the dGPS software used (EZSurv version 3.98.374 from Effigis Geo Solution), but absolute positioning accuracy depends on the PPP result from the base station (X, Y, Z) = (2, 3, 5 cm). The absolute positioning error matters when two sets of measurements are compared, e.g., to differentiate two DSMs, whereas relative positioning refers to the accuracy within each set. For example, the accuracy of GCPs specified in Agisoft Photoscan during the DSM calculation is relative to positioning. The absolute accuracy on the other hand would impact the overall error of the snow depth map.

One major issue is the link to the absolute accuracy of the base station. For winter and summer flights, the base station was not set on the same point, which led to more uncertainties in positioning. A rod was driven into the ground to create a static point for future field campaigns. The risk that the rod will rise from cryoturbation remains low in this area. It will be important to set up the base station for winter and summer flights on this point so that the absolute error in positioning can be

Table 5: DSM description for summer and winter flights. Both flights were in manual mode.

DSM	UAV	Flight		
Snow (winter)	BlitzRCWorks Sky Surfer Pro Fixed wing	Mode : Manual Zone : 40 000 m <sup>2</sup>	Nb images	548
			Resolution (DSM)	6 cm
			Altitude	20-50 m
Flight	1	Date	Area (m <sup>2</sup> )	
	2	2018-04-23	20 000	
		2018-04-26	20 000	
Snow off (summer)	DJI Phantom 3 Professional Multi rotor	Mode : Manual Zone : 40 000 m <sup>2</sup>	Nb images	709
			Resolution (DSM)	4 cm
			Altitude	50 m
Flight	1	Date	Area (m <sup>2</sup> )	
	2	2018-07-11	10 000	
		2018-07-17	10 000	
	3	2018-07-25	20 000	

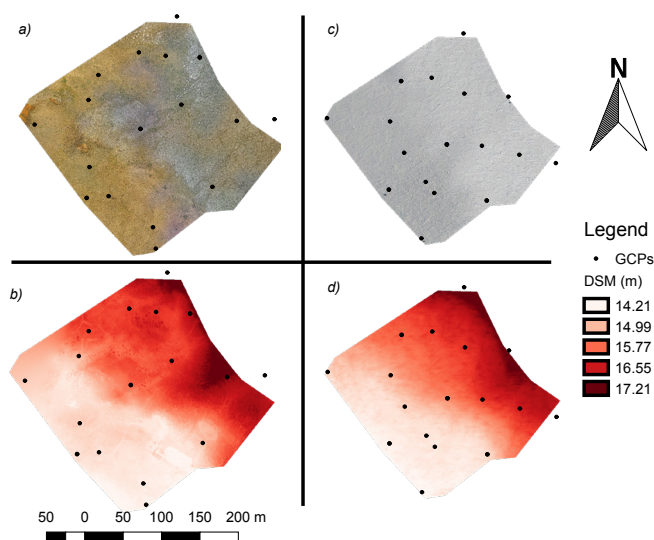


Figure 7: Orthophoto and DSM images of the study site near Cambridge Bay (69°13'19.66" N, 104°53'54.91"W). The upper left (a) shows the orthophoto from the summer flight with more vegetation on the left and more rocks on the right. The lower left (b) shows the resulting DSM from the summer flight. On the right side (c) and (d) show the orthophoto and DSM results for the winter flights.

eliminated. A correction had to be made by adding 10 cm to winter DSM from a known snow free zone that had negative snow depth. The snow free zone was barely covered by snow, but rocks were clearly visible. This small area had an average snow depth of -13 cm, so a 10 cm correction was applied to the entire snow depth map (i.e., winter DSM). Again, because the base station was not set on the same point, this offset is also on the same order of magnitude if the uncertainty of the two points ( $z = 5$  cm) from the PPP result are added. With a snow free zone, one can improve co-registration of both DSMs (Nolan et al., 2015).

A total DSM was constructed by merging multiple flight zones surveyed over two to three days (see Table 5). Conducting validation measurements from snow probing is time consuming and they were done immediately after each flight, limiting the number of flights per day. Dates for the different flight can be found in Table 5. Different light conditions are not optimal as they induce an error in the 3D reconstruction process from the

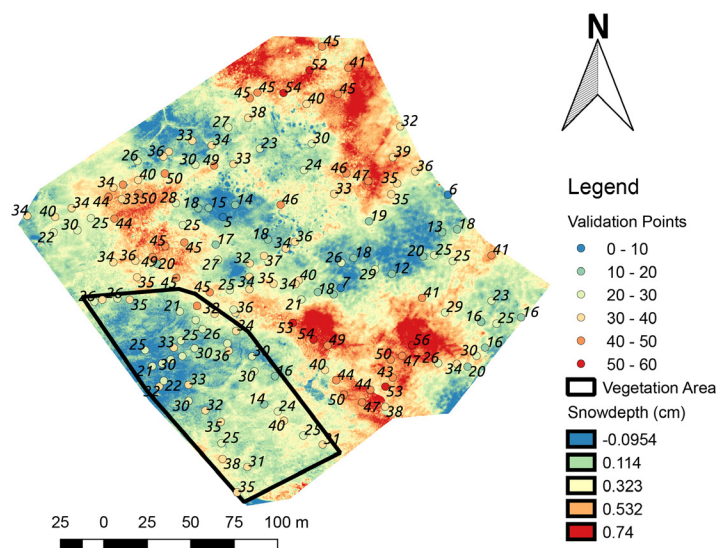


Figure 8: Snow depth map resulting from the SfM approach. The delimited area in black shows negative results due to the influence of the vegetation.

SfM workflow and must be considered. Manual measurements of snow depth were conducted for validation of the DSM using an avalanche probe, geolocated with the dGPS antenna. Notably, the typical hand-held GPS of new devices, like the Magnaprobe (Sturm, 2018), do not have a sufficient X, Y, Z precision since the DSM pixel size is approximately 5 cm. These measurements were done with an avalanche probe paired with the same dGPS system used for the GCPs. This provides excellent correspondence between validation points and the map derived by UAV. Given the very high spatial variability of snow depth and the pixel resolution of approximately 4 to 6 cm retrieved from the SfM approach, such a precision is essential. In total, 155 validation points (see Figure 8) were taken and are spread throughout the mapped area of 40 000 m<sup>2</sup>. For more information on the study site see Appendix B.

## Results and discussion

Agisoft Photoscan was used to process all images. Figure 7 shows both the DSM and the orthophoto of snow-on and snow-off conditions. The resolution of the DSM is 4 cm for the summer flight and 6 cm for winter flight. A total of 18 GCPs (see Figure 7)

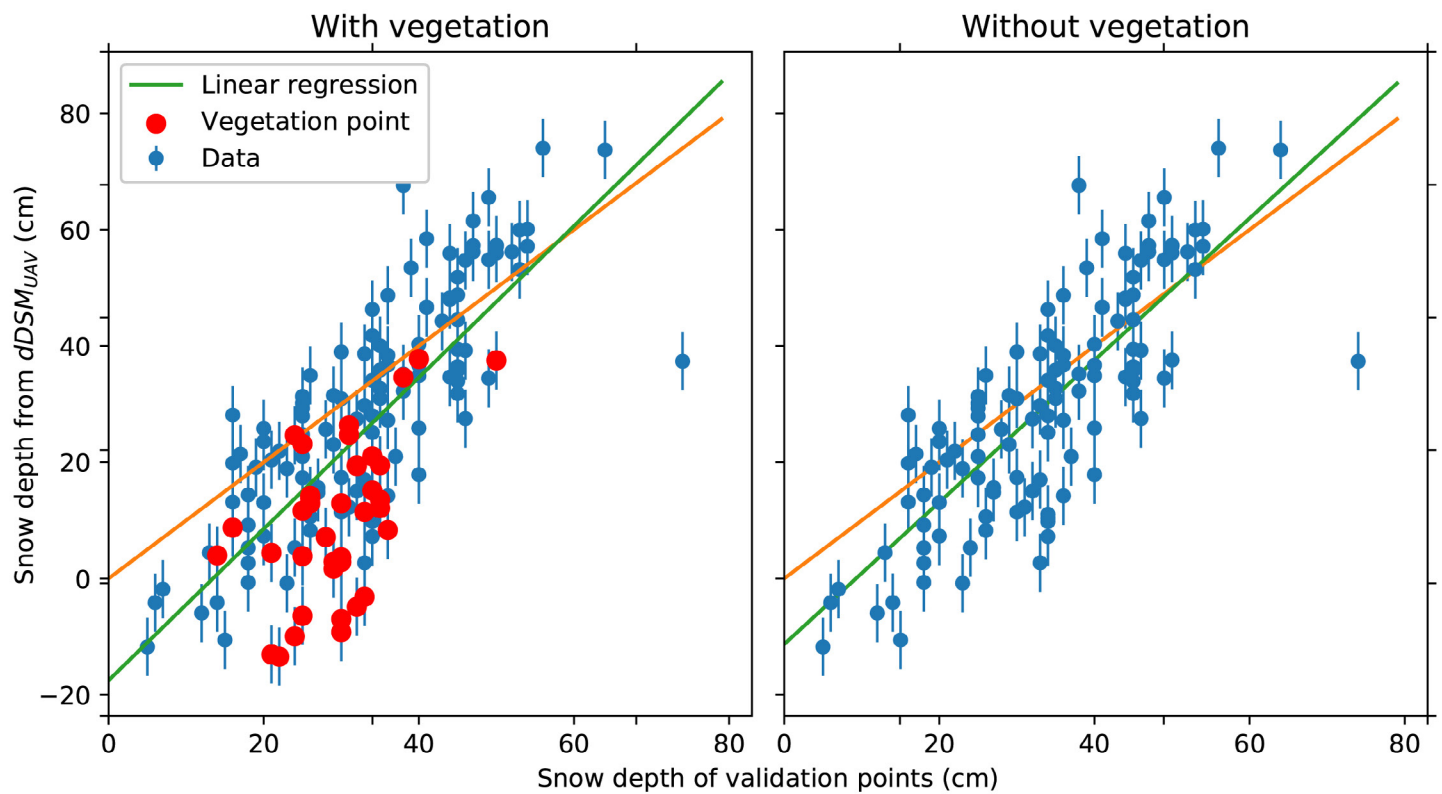


Figure 9: Regression between the snow depth validation points and the UAV derived snow depth points.

were used for optimizing camera parameters and positions. No GCPs were available for external validation so it is not possible to provide an external estimation of the precision of the DSM. The error per GCP is 8 cm on average (see appendix D) and is therefore intrinsic to the optimization because it reduces the difference between the true position of GCP and GCP position on the point cloud by optimizing camera parameters (more details on GCPs can be found in Appendix A and D). In the future, the DIY UAV design will feature

Table 6: Linear regression parameters and RMSE from snow depth validation points.

	With Vegetation	Without Vegetation
a	1.30	1.22
b	-18	-11
No. of points	155	118
RMSE	16 cm	13 cm
R2	0.57	0.64
p-value	2.14 e-30	1.66 e-27

a dGPS system that will provide fixed solution (real-time kinematic precision) for all pictures taken during flight. This will allow use of most GCPs for evaluating the precision of the DSM and leave 3 to 4 GCPs for optimization (if needed). This is necessary to maximize the precision and robustness of the DSM and to detect systematic errors (James et al., 2017; Goetz et al., 2018).

In Figure 7 (a), a zone of vegetation can be seen on the west and rockier ground on the east. The vegetation can be characterized by shrubs and sedges, more specifically *Salix richardsonii* and *Carex aquatilis*. This impacts the precision of the snow depth map as highlighted in Figure 8. The uncertainty arises from snow compaction on vegetation where the DSM summer surface (i.e., vegetation surface) is lower under compacted snow. This is in agreement with higher RMSE values recorded by Nolan et al., (2015) and Bühler et al., (2016) in vegetated areas. As for the winter DSM, there is clear influence of the wind on the snow, leading to compacted snow drifts (see Appendix C for full size orthophoto). These snow drifts provide

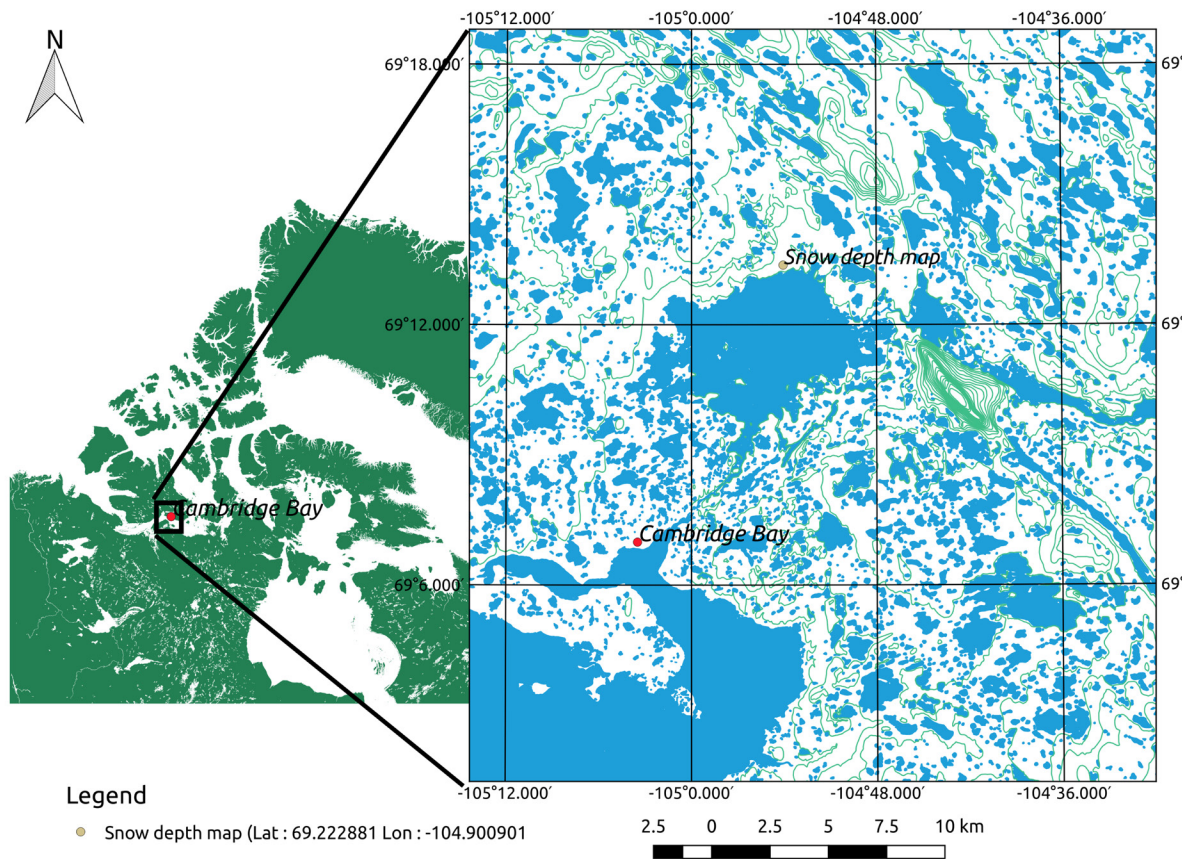


Figure 10: Map of study site at Greiner Lake Watershed.

a lot of contrast to the picture and make it easier to detect points in multiple images, even though the pictures are mostly white. Some GCPs appear to be outside of the DSM/orthophoto (Figure 7). This is an artificial effect, as only the regions with enough overlap between pictures are used for creating the DSM. The overlap between both DSMs is equivalent

to the snow depth map (see Figure 8). Also shown in Figure 8, there are 155 validation points, with an average of 33 cm snow depth.

Figure 9 shows the comparison between snow depth from validation points and from the dDSM\_UAV map. The orange line represents the best

Table 7: Camera parameters used in both winter and summer DSMs.

Camera	Mode	Sensor	FOV	Resolution
GoPro 6 (winter DSM)	normal	1/2.3" cmOS	122°	Photo: 12 MP Video: 8 MP
	linear		85°	Photo: 8 MP Video: 5 MP
DJI Phantom 3 Professional (summer DSM)	normal	1/2.3" cmOS	94°	12 MP
Sony a6000 (future work)	normal	23.50 mm x 15.60 mm cmOS	73°	24 MP

correspondence between validation points and the UAV map. Validation points over vegetation are marked in red and were removed on the second graph in Figure 9. Vegetation areas were identified using a combination of photographs from the DIY UAV design and ground observations. It can be seen in Table 6 that these vegetation points have an impact on the correlation and the RMSE. Overall, the RMSE is 16 cm, which is comparable to the literature.

Compared to work in alpine regions or tundra environments, the arctic snowpack near Cambridge Bay is rather small with an average of 33 cm, measured in early spring (April 2018). Therefore, micro-topography and vegetation have a stronger influence on the map accuracy. Improvements are possible for Global Navigation Satellite System handling and processing (as explained above) with the 10 cm off correction applied to the winter DSM. Further improvements will also be possible by switching from manual flights to automated flights, as a constant altitude and constant overlap will increase the uniformity of the point cloud. Additionally, setting the camera to fixed camera parameters and flying zones on the same day will give constant light conditions and reduce reconstruction uncertainties of the point cloud (Bühler et al., 2017). A higher-resolution camera will also be tested for better DSM results (see Appendix A for camera info).

## Conclusions

This project aimed to build an aircraft capable of flying in winter conditions in the North, as such the focus was on material testing for cold temperatures. Batteries and electronics were tested at various temperatures to understand their limitations before using them in the field. Initially, there were no battery preferences. For the experiments, different sized and shaped batteries were purchased for use in this project and others, such as powering the radar system. Being able to have a variety is beneficial, and allows for battery selection based on mission requirements. The fixed-wing DIY UAV designs are close to their

maximum payload, so somewhat smaller batteries are preferred on these missions. In contrast, the yet-to-be-built quadcopter will benefit from more lifting capacity, so the battery size will matter less.

Currently, an additional Finwing Penguin aircraft has been purchased. It has a stronger engine than the BlitzRCWorks Skysurfer Pro, was easier to fly in wind, and was easier to prepare and maintain in the field. The next steps will include designing and building a quadcopter for the radar system. It currently requires a system capable of relatively low and slow flight. While a glider can provide the later, low flights (under 5 m) are too risky. Additionally, the hovering ability will make it easier to aim for nadir measurements. Small deviations will occur and the research team will have to decide whether to counter them with a gyroscope or an electronic accelerometer. The latter has the benefit of being lighter, the former of actually achieving nadir. In addition, working more frequently on the X-UAV Talon platform will allow future flights in higher wind speeds.

In terms of scientific applications, the next intuitive step is to add a Normalize Difference Vegetation Index (NDVI) layer to the snow depth map. This will establish an empirical relationship between snow depth bias and vegetation type. This could also lead to a finer scale analysis of snow-shrub interaction (Sturm et al., 2001). Furthermore, an analysis of micro-topography is planned using a topographic index, such as an upwind slope index, with dominant wind to better understand the snow redistribution processes (Winstral et al., 2002). This can be useful in soil thermal applications. This type of map is rather rare in the Arctic given all the logistical constraints highlighted in this work. Despite the scarcity of the available data to date, future snow depth information at high resolution will be beneficial for hydrology (melt timing, geochemical processes), permafrost (active layer monitoring) and ecology (habitat characterization). Many physical processes at this level influence larger-scale processes, and detailed snow distribution maps could be used to analyze sub-pixel variability of snow models or surface state

retrievals (i.e., snow water equivalent) derived from coarse resolution satellite imagery.

## Acknowledgements

The authors would like to thank David Rancourt and Alexis Lussier-Desbiens for their training and support in building and modifying our frames. Their knowledge and experience in UAV design contributed significantly to the success of our flights. This project was funded through Polar Knowledge Canada, the National Science and Engineering Research Council for Canada, and the Fonds Québécois de la recherche sur la nature et les technologies. Special thanks to the staff of the Canadian High Arctic Research Station and the community of Cambridge Bay, Nunavut, for their tremendous logistical support during the field campaigns.

## Appendix A

Description of both cameras used for the snow depth map. The GoPro 6 had to be used in linear mode to avoid the fish-eye distortion from these type of action cameras which reduced the resolution. Videos were also recorded and tested (instead of photographs) while flying which led to a loss of spatial resolutions and much heavier post-processing.

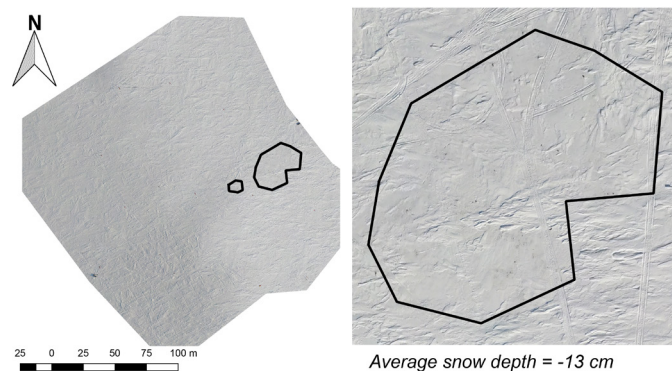


Figure 11: Orthophotos from the April flights.

Markers	Easting (m)	Northing (m)	Altitude (m)	Accuracy (m)	Error (m)	Projections	Error (pix)
<input checked="" type="checkbox"/> 101	503990.002000	7679155.692000	14.802000	<b>0.005/0.012</b>	0.028189	11	0.365
<input checked="" type="checkbox"/> 102	503924.449000	7679084.147000	14.112000	<b>0.005/0.012</b>	0.048929	12	0.767
<input checked="" type="checkbox"/> 103	503921.187000	7679108.808000	14.281000	<b>0.005/0.012</b>	0.058068	14	0.515
<input checked="" type="checkbox"/> 104	503869.852000	7679144.885000	14.388000	<b>0.005/0.012</b>	0.225831	10	0.589
<input checked="" type="checkbox"/> 105	503844.497000	7679142.810000	14.362000	<b>0.005/0.012</b>	0.111675	13	0.335
<input checked="" type="checkbox"/> 106	503906.737000	7679222.762000	15.545000	<b>0.005/0.012</b>	0.055086	4	0.135
<input checked="" type="checkbox"/> 201	503844.516000	7679142.837000	14.365000	<b>0.006/0.016</b>	0.118750	12	0.257
<input checked="" type="checkbox"/> 202	503906.727000	7679222.769000	15.551000	<b>0.005/0.006/0....</b>	0.050462	16	0.255
<input checked="" type="checkbox"/> 203	503847.647000	7679178.554000	14.611000	<b>0.006/0.007/0....</b>	0.029599	11	0.399
<input checked="" type="checkbox"/> 204	503784.159000	7679227.752000	14.868000	<b>0.006/0.007/0....</b>	0.106292	13	0.387
<input checked="" type="checkbox"/> 205	503846.518000	7679256.293000	15.020000	<b>0.006/0.007/0....</b>	0.148801	13	0.166
<input checked="" type="checkbox"/> 206	503857.960000	7679285.157000	15.722000	<b>0.006/0.007/0....</b>	0.083373	11	0.321
<input checked="" type="checkbox"/> 307	503904.894000	7679311.262000	16.051000	<b>0.006/0.007/0....</b>	0.065924	11	0.424
<input checked="" type="checkbox"/> 308	503949.014000	7679352.993000	17.370000	<b>0.005/0.006/0....</b>	0.027096	10	0.326
<input checked="" type="checkbox"/> 309	503935.949000	7679307.399000	16.135000	<b>0.005/0.006/0....</b>	0.080173	14	0.435
<input checked="" type="checkbox"/> 310	503975.339000	7679305.502000	16.586000	<b>0.005/0.006/0....</b>	0.056571	18	0.146
<input checked="" type="checkbox"/> 403	503954.077000	7679250.819000	15.961000	<b>0.005/0.012</b>	0.034524	11	0.311
<input checked="" type="checkbox"/> 404	504018.222000	7679231.977000	16.939000	<b>0.005/0.013</b>	0.024358	27	0.179
<input checked="" type="checkbox"/> 405	503975.348000	7679305.466000	16.591000	<b>0.005/0.012</b>	0.063655	30	0.198
<input checked="" type="checkbox"/> 406	504061.918000	7679233.983000	16.859000	<b>0.005/0.013</b>	0.069560	13	0.240
<b>Total Error</b>							
Control points					0.088421		0.353
Check points							

Figure 12: Detailed GCP information from summer DSM.

## Appendix B

Here is a map that shows the study site in Cambridge Bay, Nunavut, Canada. More specifically, the study site is located in Greiner Lake Watershed.

## Appendix C

Overview of the orthophotos for the April flights where snow spatial patterns caused by wind can be observed. The zone in black is the snow free zone used to apply the 10 cm correction explained in the section on snow depth retrieval application.

## Appendix D

Ground control points with their position accuracy related to the GPS system and the difference (Error (m)) between the position and the 3D model. Only summer GCPs are shown since winter and summer accuracy is similar.

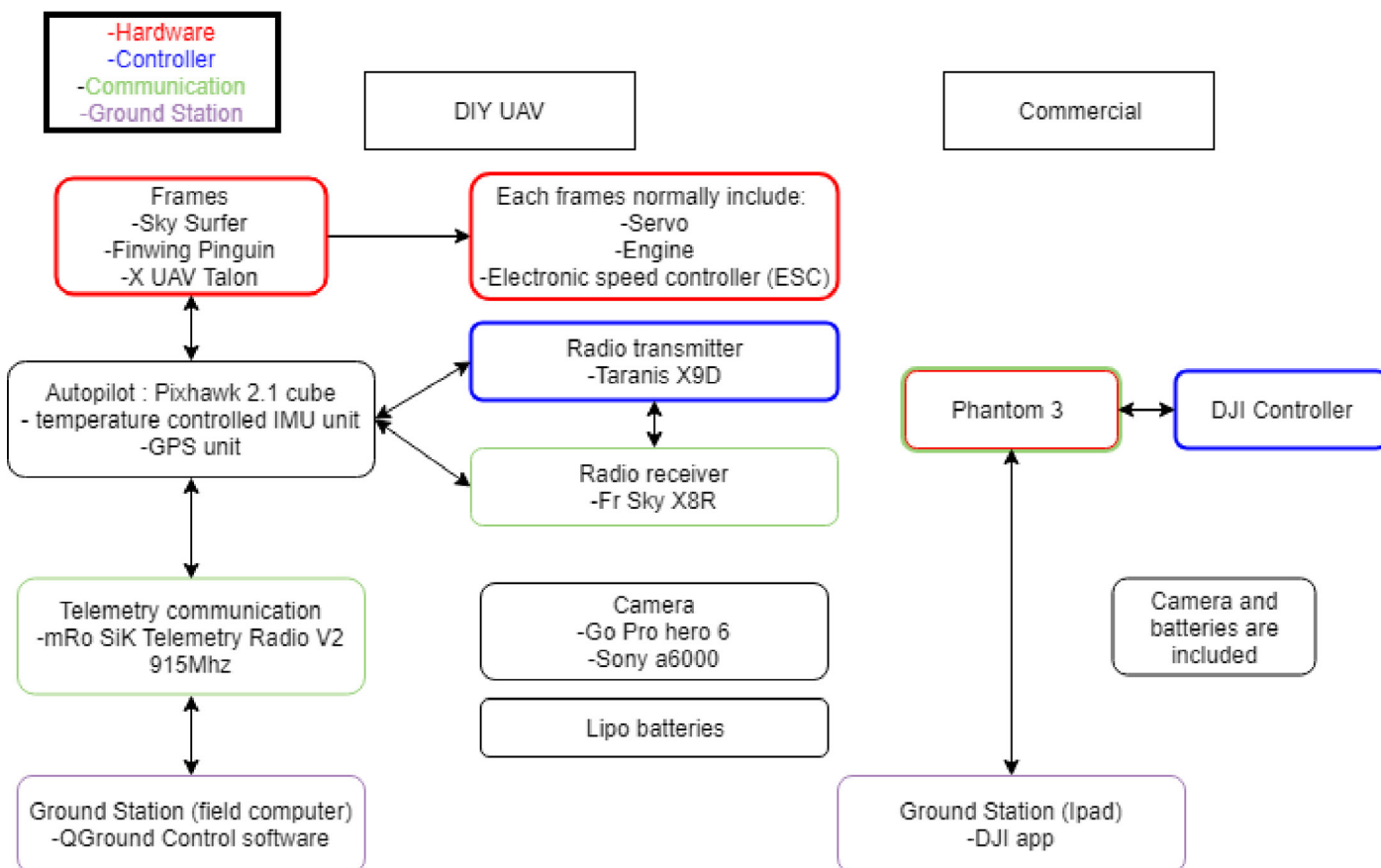


Figure 13: DIY system design components (left) versus commercial components (right).

## Appendix E

The components in the DIY UAV system design can be separated into two different categories:

1. Mechanic, the frame is the actual UAV itself (in this case the type is a fixed-wing frame); and
2. Electronic, all the electronics inside (related to the autopilot).

One of the advantages of the DIY-approach is that you can re-use and cross-use the electronics for different UAVs (including fixed- and rotary-wing).

## References

Abdilla, A., Richards, A., Burrow, S. 2015. Power and Endurance Modelling of Battery-Powered Rotorcraft. IEEE/RSJ International Conference on Intelligent Robots and Systems (IROS).

- Ader, M., Axelsson, D. 2017. Drones in Arctic Environments. Master thesis, KTH Royal Institute of Technology, Stockholm, Sweden.
- Anderson, K., Westoby, M.J., James, M.R. 2019. Low-budget topographic surveying comes of age: Structure from motion photogrammetry in geography and the geosciences. *Progress in Physical Geography: Earth and Environment*, 43(2):163–173. Retrieved from: <https://doi.org/10.1177/0309133319837454>.
- Bühler, Y., Adams, M.S., Bosch, R., Stoffel, A. 2016. Mapping snow depth in alpine terrain with unmanned aerial systems (UASs): Potential and limitations. *The Cryosphere*, 10(3):1075–1088.
- Bühler, Y., Adams, M.S., Stoffel, A., Boesch, R. 2017. Photogrammetric reconstruction of homogenous snow surfaces in alpine terrain applying near-infrared UAS imagery. *International Journal of Remote Sensing*, 38(8-10):1–24.
- Chudley, T.R., Christoffersen, P., Doyle, S.H., Abellan, A., Snooke, N. 2019. High-accuracy UAV photogrammetry of ice sheet dynamics with no ground control. *The Cryosphere*, 13(3):955–968. Retrieved from: <https://doi.org/10.5194/tc-13-955-2019>.
- Cimoli, E., Marcer, M., Vandecrux, B., Bøggild, C.E., Williams, G., Simonsen, S.B. 2017. Application of Low-Cost Uass and Digital Photogrammetry for High-Resolution Snow Depth Mapping in the Arctic. *Remote Sensing*, 9(11):1–29. Retrieved from: <https://doi.org/10.3390/rs9111144>.
- De Michele, C., Avanzi, F., Passoni, D., Barzaghi, R., Pinto, L., Dosso, P., Ghezzi, A., Gianatti, R., Della Vedova, G. 2016. Using a fixed-wing UAS to map snow depth distribution: An evaluation at peak accumulation. *The Cryosphere*, 10:511–522.
- DJI. 2015. Phantom 3 Professional, User manual.
- Eckerstorfer, M., Solbø, S., Malnes, E. 2015. Using “Structure-from-Motion” Photogrammetry in Mapping Snow Avalanche Debris. *Wiener Schriften zur Geographie und Kartographie*, 21:171–178.
- Fernandes, R., Prevost, C., Canisius, F., Leblanc, S.G., Maloley, M., Oakes, S., Holman, K., Knudby, A. 2018. Monitoring snow depth change across a range of landscapes with ephemeral snowpacks using structure from motion applied to lightweight unmanned aerial vehicle videos. *The Cryosphere*, 12(11):3535–3550.
- Goetz, J., Brenning, A., Marcer, M., Bodin, X. 2018. Modeling the precision of structure-from-motion multi-view stereo digital elevation models from repeated close-range aerial surveys. *Remote Sensing of Environment*, 210:208–216.
- Granshaw, S.I. 1980. Bundle adjustment methods in engineering photogrammetry. *The Photogrammetric Record*, 10:181–207.
- James, M.R., Robson, S., d’Oleire-Oltmanns, S., Niethammer, U. 2017. Optimising UAV topographic surveys processed with structure-from-motion: Ground control quality, quantity and bundle adjustment. *Geomorphology*, 280:51–66.
- Jo, D., Kwon, Y. 2019. Development of Autonomous VTOL UAV for Wide Area Surveillance. *World Journal of Engineering and Technology*, 7(1):227–239. Retrieved from: <https://doi.org/10.4236/wjet.2019.71015>.
- Langlois, A., Royer, A., Goïta, K. 2010. Analysis of simulated and space-borne passive microwave brightness temperatures using in situ measurements of snow and vegetation properties. *Can. J. Remote Sensing*, 36(1):S135–S148.
- Lowe, D.G. 2004. Distinctive image features from scale invariant keypoints. *International Journal of Computer Vision*, 60(2):91–110.

Mulgaonkar, Y., Whitzer, M., Morgan, B., Kroninger, C.M., Harrington, A.M., Kumar, V. 2014. Power and weight considerations in small, agile quadrotors. SPIE Defense+ Security, pp. 90831Q–90831Q, International Society For Optics and Photonics.

Murtiyoso, A., Koehl, M., Grussenmeyer, P., Freville, T. 2017. Acquisition and processing protocols for UAV images: 3D modeling of historical buildings using photogrammetry. ISPRS Annals of the Photogrammetry, Remote Sensing and Spatial Information Sciences, 4:163–170.

Nolan, M., Larsen, C., Sturm, M. 2015. Mapping snow depth from manned aircraft on landscape scales at centimeter resolution using structure-from-motion photogrammetry. *The Cryosphere*, 9:1445–1463.

Pomerleau P. 2016. Conception d'un dispositif de caractérisation de la glace et de la neige à partir d'un radar à émission continue. Masters thesis, Université de Sherbrooke.

Rutter, N., Sandells, M., Derksen, C., Toose, P., Royer, A., Montpetit, B., Langlois, A., Lemmetyinen, J., Pulliainen J. 2014. Snow stratigraphic heterogeneity within ground-based passive microwave radiometer footprints: Implications for emission modeling. *Journal of Geophysical Research: Earth Surface*, 119(3):550–565. doi:10.1002/2013JF003017.

Salerno, D., Korsunsky R. 1998. Practical considerations in the design of lithium-ion battery protection systems. APEC '98 Thirteenth Annual Applied Power Electronics Conference and Exposition, IEEE. doi: 10.1109/APEC.1998.653975.

Sturm, M. 2018. An Automatic Snow Depth Probe for Field Validation Campaigns. Technical Reports, 9695–9701.

Sturm, M., McFadden, J.P., Liston, G.E., Chapin III, F.S., Racine, C.H., Holmgren, J., Stuart Chapin, F., Racine, C.H., Holmgren, J. 2001. Snow-Shrub Interactions in Arctic Tundra: A Hypothesis with Climatic Implications. *Journal of Climate*, 14(3):336–344.

Turner, D., Lucieer, A., de Jong, S.M. 2015. Time series analysis of landslide dynamics using an Unmanned Aerial Vehicle (UAV). *Remote Sensing*, 7(2):1736–1757.

Wang, Q. 2015. Analysing and evaluating a thermal management solution via heat pipes for lithium-ion batteries in electrical vehicles. PhD thesis, University of Nottingham.

Winslow, J., Benedict, M., Hrishikeshavan, V., Chopra, I. 2016. Design, development, and flight testing of a high endurance micro quadrotor helicopter. *International Journal of Micro Air Vehicles*, 8(3):155–169. doi: 10.1177/1756829316653694.

Winstral, A., Elder, K., Davis, R.E. 2002. Spatial Snow Modeling of Wind-Redistributed Snow Using Terrain-Based Parameters. *Journal of Hydrometeorology*, 3:524–538.